Astron. Astrophys. 249, 75–87 (1991)

ASTRONOMY AND ASTROPHYSICS

CCD surface photometry of the low-luminosity radio galaxies containing radio jets B2 0034+25 and B2 0206+35⋆

J.I. González-Serrano[1] and I. Pérez-Fournon[2]

[1] Departamento de Fisica Moderna, Universidad de Cantabria, Avda. de los Castros s/n, E-39005 Santander, Spain
[2] Instituto de Astrofisica de Canarias, E-38200 La Laguna, Tenerife, Spain

Received November 30, 1990; accepted February 18, 1991

Abstract. We present broad-band CCD imaging of the radio galaxies B2 0034+25 and B2 0206+36. Both galaxies are of low radio power and contain radio jets at the arcsec scale. The galaxies have close companions and the optical morphology suggests that they are interacting. The surface photometry method and its application to interacting galaxies is described. It involves the following steps: 1) isophotal ellipse fitting of the main galaxy after semi-automatic deletion of interfering images, 2) construction of a quasi-elliptical model of the main galaxy from the best-fit parameters, 3) subtraction of the model from the original image. These steps are applied consecutively to each companion galaxy. An estimate of the photometric accuracy is obtained by applying this method to realistic simulations of galaxy pairs. This technique is found to be a powerful tool for studying galaxy interactions allowing the detection of photometric effects of the interaction such as non-concentric isophotes and deviations of the galaxy surface brightness profiles in the outer parts from the extrapolation of a de Vaucouleurs law fitted to the inner parts of the galaxy. In particular the two objects discussed in this paper appear to be strongly interacting with nearby companions. We estimate lower limits for the radio-to-optical spectral indices of the jets and conclude that the optical emission from the inner parts of the jets lies below a power-law extrapolated from radio wavelengths. The role of hot gas around elliptical galaxies on the collimation of the radio jets is briefly discussed.

Key words: galaxies: B2 0034+25, B2 0206+35 – jets of galaxies – radio galaxies – structure of galaxies – elliptical galaxies – photometry

1. Introduction

In the last few years several CCD imaging studies of powerful radio galaxies (PRG) have reactivated the interest in this type of objects as a method to understand the origin of nuclear activity in elliptical galaxies. Heckman et al. (1986) found that a large fraction of powerful radio galaxies have a complex optical morphology. Many of them appear to be interacting with nearby companions and show distorted isophotes or filamentary structure. An extensive broad-band imaging survey of powerful radio galaxies has been undertaken by Smith & Heckman (1989a, b). They found that a high fraction of PRG show deviations from elliptical isophotes at high levels of surface brightness. The fact that about half of PRG with strong emission line spectra display peculiar morphologies is interpreted by the authors as an effect of galaxy interactions involving gas-rich (disk) galaxies.

Narrow-band emission line imaging of these objects shows that a relatively high percentage of the galaxies studied have extranuclear emission line regions (Baum & Heckman 1989a; Fosbury 1989). The luminosity and spatial distribution of the extended narrow line regions is correlated with the radio luminosity and morphology (Baum & Heckman 1989b). These studies have concentrated on objects which populate the brightest end of the radio luminosity function and therefore are only representative of the most powerful objects and not of the more common intermediate- and low-luminosity objects.

It is well known that the radio morphology is related to total radio power. Low luminosity objects (of total radio power at 1.4 GHz less than 10^{25} W Hz^{-1}) present, in general, a Fanaroff-Riley (1974) type I radio structure, while objects of radio power higher than that limit usually present a Fanaroff-Riley type II morphology with edge-brightened lobes. Low-luminosity radio galaxies usually present jets on both sides of a weak core while jets in high-luminosity radio galaxies tend to be faint relative to the core. Therefore, the observations of powerful radio galaxies are not very suited to the study of the physics of extragalactic jets. Also, low-luminosity radio galaxies inhabit regions of higher galaxy density than those occupied by high-luminosity objects (Longair & Seldner 1979; Stocke 1979; Lilly & Prestage 1987; Prestage & Peacock 1988).

Motivated by all these facts we have started an optical study, including CCD imaging of low-luminosity radio galaxies. Since our main initial aim was the detection of optical counterparts of radio jets, we restricted our sample to low-luminosity radio galaxies with well defined radio jets. In this paper we describe the surface photometry procedure used and we apply this method to study the optical counterparts of B2 0034+25 and B2 0206+35. The capability of the procedure in order to obtain the galaxy

Send off print requests to : J.I. González-Serrano

⋆ Based on observations made with the Isaac Newton Telescope operated by the Royal Greenwich Observatory at the Spanish Observatorio del Roque de los Muchachos of the Instituto de Astrofisica de Canarias on behalf of the Science and Engineering Research Council of the United Kingdom and the Netherlands Organization for Scientific Research (NWO).

parameters, and the accuracy of the measured parameters is studied by simulating CCD images of elliptical galaxies.

Colina & Pérez-Fournon (1990a, b) describe a related study of low- and intermediate-luminosity radio galaxies selected from the Bridle & Perley (1984) list of radio-jet galaxies and quasars.

The structure of the paper is as follows. Sect. 2 presents a detailed description of the data reduction and photometric methods. It includes the method to estimate the photometric accuracy based on the application of the ellipse-fitting programs to realistic simulations of pairs of elliptical galaxies. Sect. 3 gives the basic optical properties of the radio-jet galaxies B2 0034+25 and B2 0206+35 and their companions and Sect. 4 discusses these results in terms of close galaxy encounters and the effect of the galaxy atmospheres on the morphology and collimation of the radio emission. We calculate lower limits to the radio-to-optical spectral indices of the jets which are compared to the spectral indices at radio wavelengths.

2. Observations and data reduction

2.1. Observations and initial data reduction

The galaxies studied here belong to the complete list of radio galaxies with jet-like structures at the arcsec scale (Parma et al. 1987). These B2 radio galaxies were originally selected for observations with the VLA from two lists of B2 objects associated with galaxies: a bright sample (Colla et al. 1975) and a faint one (Fanti et al. 1978). The first sample is formed by B2 sources identified with galaxies listed in the Zwicky Catalogue of Galaxies and Clusters of Galaxies and the faint one contains B2 objects identified with galaxies brighter than 17th mag on the Palomar Observatory Sky Survey. Based on these criteria, the sample is considered to be statistically complete. Although the B2 radio-jet sample is not defined in terms of radio luminosity, all objects are of low radio power. The total power of the sources is less than 10^{25} W Hz^{-1} at 1.4 GHz and the absolute optical magnitude M is $-19 > M > -23$.

B2 0034+25 and B2 0206+35 were observed with the Prime Focus CCD camera (RCA chip) of the Isaac Newton Telescope on 1987 October 18. The pixel size and field of view were 0.″74 × 0.″74 and 3.′95 × 6.′31, respectively. For both galaxies a 180 s exposure in a KPNO V filter and a 20 min exposure in a filter of 53 Å FWHM isolating the redshifted Hα+[N II] λ6584 lines were obtained under photometric observing conditions. The absolute calibration of the V frames was done from observations of the open clusters NGC 2419 and NGC 7790 (Christian et al. 1985). The correction for galactic extinction was calculated following Huchra (1977) and Savage & Mathis (1979). The seeing was in the range 1.″3–2″ FWHM.

The images were bias subtracted and flat-fielded using exposures of the twilight sky and of the dome illuminated by a tungsten lamp. The flat-field correction was found to be good to 0.5%. Cosmic ray hits were removed from each image.

The wide field of the INT Prime Focus CCD images, and the relatively high redshift of the B2 radio galaxies when compared with bright nearby massive ellipticals, allows us to make a good determination of the sky background. The sky level in each frame was calculated using three different methods: 1) mode of the distribution of pixel values along the edge of the frame (width of ~30″), 2) average of mean values in boxes in regions of the CCD images distant from the galaxy and free of interfering objects, and 3) the asymptotic value of the galaxy+sky brightness profile obtained as described below. These three values agree to better than 1%.

2.2. Ellipse fitting

Over the last few years several groups have demonstrated the usefulness of photometric methods based on fitting ellipses to the isophotes for the study of elliptical galaxies. Two main procedures have been developed: a) proper least-square ellipse fits to the isophotes (Bender & Möllenhoff 1987), and b) study of the intensity variations along elliptical contours fitted to the galaxy intensity distribution. Although the two methods are different, their parametrization of the isophote shapes of elliptical galaxies is similar. Deviations from ellipticity can be studied by analyzing the radial deviations of the isophote from the best-fit ellipse or the intensity variations along the best-fit ellipse as a Fourier series. The procedure for ellipse-fit analysis that we have developed is based on the program PROF of the GASP galaxy surface photometry package, written by M. Cawson (1983) at Cambridge and used extensively by other groups (e.g. Jedrzejewski 1987; Smith & Heckman 1989a, b; Peletier 1989). The basic differences of our method, as opposed to the original Cawson programmes, are that interfering objects are identified by a semi-automatic procedure and that a single program makes the ellipse-fit and the study of the Fourier coefficients describing non-ellipticities of the isophotes.

2.3. Simulations of elliptical galaxies and photometric accuracy

The most common method generally used to establish the accuracy of CCD surface photometry of elliptical galaxies is the comparison of the parameters describing the isophote shapes (ellipticity, P.A., and surface brightness as a function of semi-major axis or equivalent radius) with independent CCD or photographic data. One obvious drawback of this comparison is that the errors of both sets of data add up in the subtraction. We have preferred to simulate elliptical galaxies with a known de Vaucouleurs surface brightness profile, and given ellipticity and position angle using GASP program SIMGAL. SIMGAL generates a data frame with a known luminosity profile to test the reduction techniques and for comparison with real images. The background intensity level and noise of the simulated images were set to reproduce the data obtained with the INT Prime Focus camera.

We have analysed two isolated elliptical galaxies which were added afterwards in order to simulate a galaxy pair. Table 1 gives the basic parameters used. The isophotes are also assumed to be concentric, and of constant ellipticity and position angle.

2.3.1. Isolated galaxies

The photometric accuracy of the parameters for isolated galaxies with no interfering images was calculated by comparing these results with the input parameters given in Table 1. We measured the mean value of the difference between the parameters obtained with PROF and the input ones. In order to avoid errors due to interpolation at small radii (see Jedrzejewski 1987) this was done for values of the semimajor axis larger than 5 pixels (3.″7). The outer semimajor axis used in this calculation was that for which

Table 1. Parameters of simulated galaxies

Galaxy	μ_e	r_e (″)	Ellipticity	P.A. (°)	Separation (″)
A	23.0	42.0	0.1	160	—
B	21.5	10.5	0.1	220	42 SE

the deviations in intensity were larger than 30%. The results for all the fitted parameters are the following:

Position angle (*P.A.*). The mean of the deviations from the input P.A. is 0. The mean dispersion is 1.5°. This indicates that PROF is able to measure with high accuracy the isophote position angle, even for very low CCD count levels and relative round galaxies.

Ellipticity. Again, the mean of the deviations from the input ellipticity of 0.1 is 0. The maximum absolute deviation of ellipticity for the two individual galaxies considered here is 0.01 for the faintest galaxy, i.e. 10% of the input ellipticity. The mean dispersion is 0.005. Jedrzejewski (1987) estimates a mean dispersion of the deviations in ellipticity using two different data sets of 0.02. This is consistent with our value since we are only measuring galaxy models with known shape.

Isophote centers. The separation δ between the isophote center at a given semimajor axis a and the center of the inner isophotes is an important parametrization of nonconcentric isophotes. Lauer (1988) proposed to use the quantity δ/a as an indication of the effects of tidal interactions. While most studies of nearby ellipticals have assumed isophotes concentric with the nucleus of the galaxy, we have also fitted with PROF the position of the isophote centers (X_c, Y_c). The absolute deviation of X_c and Y_c from the input values is less than 0.03 pixels, with a mean dispersion of 0.13 pixels. δ/a is always less than 1.2%.

B_4. The amplitude of the fourth cosine Fourier component relative to the mean intensity of the contour, B_4, indicates deviations of the isophote shape from ellipticity in the form of "pointed isophotes", ($B_4>0$), or "boxy" isophotes ($B_4<0$). The relevance of this parameter for our understanding of the formation and evolution of elliptical galaxies has only recently been stressed by Bender et al. (1989), Nieto & Bender (1989) and Peletier (1989). In this simulation all Fourier coefficients should be negligible. In fact, PROF measures very low B_4 values, with a mean of 0.0007, and dispersions of 0.005 (0.5%). Jedrzejewski (1987) gives typical dispersion of B_4 of 0.0001 and 0.005 for bright and faint galaxies, respectively.

Surface brightness profile. We have fitted a de Vaucouleurs profile to our PROF profiles (intensity versus semimajor axis) and compared the measured values of effective radius (r_e) and surface brightness at that radius (μ_e) with the input ones. The deviations of r_e and μ_e from the input values are 5% and 0.05 mag/arcsec^2, respectively. We have also compared the differences between our input brightness profiles and the ones measured by PROF, finding no systematic deviations and a mean dispersion of 0.05 mag. The input profile is also well reproduced in the outer parts of the galaxies at intensity levels of less than 10 counts per pixel or $\lesssim 1.2\%$ of the sky intensity level.

2.3.2. Pairs and groups of galaxies

The investigation of the shape of the individual components of pairs or groups of galaxies is difficult when the typical separations are of order of their effective radii. One approach, proposed by Lauer (1988), is to fit simultaneously the 2-D intensity distribution by a superposition of elliptical models. A main drawback of this approach is that the galaxy centers were set to fixed values to simplify the problem.

We demonstrate below that, if one of the components of the pair dominates the total intensity distribution over a large area, it is possible to apply the method described above consecutively to the individual components of the pair obtaining a reliable parametrization of the two galaxies. We discuss here the results of applying our photometric method to the pair formed by superposition of the two galaxies discussed above, considering typical separations and relative intensities of pairs of elliptical galaxies associated to B2 radio galaxies.

Figure 1 shows a contour map of the galaxy pair. We note, that a priori it is difficult to distinguish whether the overall morphology of the system responds to the superposition of two elliptical galaxies or there is also some "common envelope" around them.

The analysis of the simulated galaxy pair proceeded as follows:

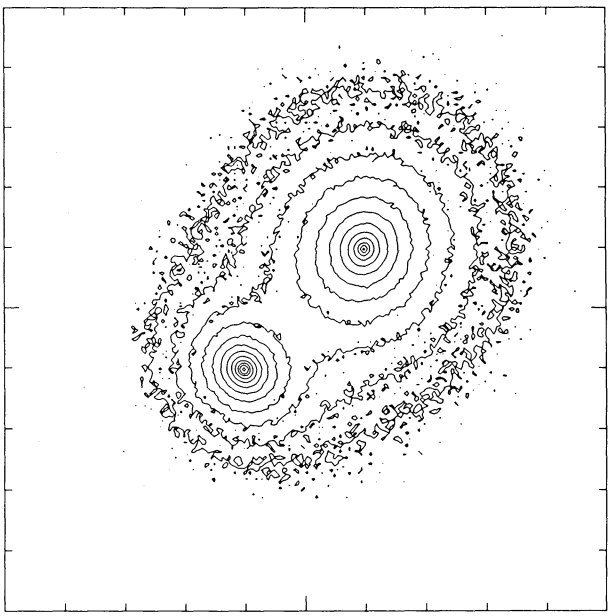

Fig. 1. Contour plot of the simulated pair of galaxies. The map corresponds to the sum of the two galaxies. The separation between contours is 0.5 mag

1) The main part of the companion galaxy and part of the region between the two galaxies where the contribution of the companion is important were masked. The distance from the center of the main galaxy (galaxy A) to the line perpendicular to the axis defined by the centers of the galaxies, where the masked region starts, was one fourth of the separation of the galaxies.

2) Elliptical contours were fitted to the valid region, starting at a semimajor axis a of 2 pixels and increasing it by 5% between consecutive fits.

3) A quasi-elliptical model of the main galaxy was constructed from the parameter files obtained in (2) and subtracted from the original image of the galaxy pair.

4) A new mask was constructed from the residual image. Similarly as before, part of the region between the two galaxies where the contribution of the main galaxy is important was masked.

5) We proceeded with the analysis of the galaxy shape of the companion galaxy in a similar way as was done for the main galaxy (step 2).

Figure 2 shows the photometric parameters calculated using PROF as a function of semimajor axis for the brightest galaxy. The fits to each galaxy are affected by some unknown contribution of light from the other component of the pair and by a lower value of the fraction of the contour used in the fits in the outer regions of the galaxies. Although strong deviations from the input parameters appear for the ellipticity and position angle in both galaxies at values of the semimajor axis larger than half the separation between the two galaxies, the deviations are not high for the inner parts of both galaxies. At a semimajor axis equal to the half light semimajor axis ($\log r_e = 1.6$), the measured ellipticity of the brightest component of the pair is ~ 0.13 and the position angle deviates from the real one by 4°. Similarly for the companion, at $a = r_e$ ($\log r_e = 1.02$) we measure an ellipticity of 0.11 and a deviation in P.A. of $\sim 4°$. Similarly, the isophote centers which should be constant, show deviations in the direction of the companion. δ/a for $a = r_e$ is 5% and 2% for galaxies A and B, respectively. Therefore, we must interpret carefully the ellipticity, P.A., and isophote center profiles at large radii. Nevertheless, an interesting result is that the deviations of the surface brightness profiles from the input ones are rather low (Fig. 2). A fit to each galaxy surface brightness profile gives the following results: for galaxy A $r_{ef} = 44''.5$ ($r_{ei} = 42''.0$), $\mu_{ef} = 23.04$ ($\mu_{ei} = 23.0$), and for the companion $r_{ef} = 10''.21$ ($r_{ei} = 10''.5$), $\mu_{ef} = 21.45$ ($\mu_{ei} = 21.5$), where subscripts f and i refer to fitted and input, respectively. Figure 3 shows the differences between the fitted de Vaucouleurs law and surface brightness. No strong deviations from the assumed de

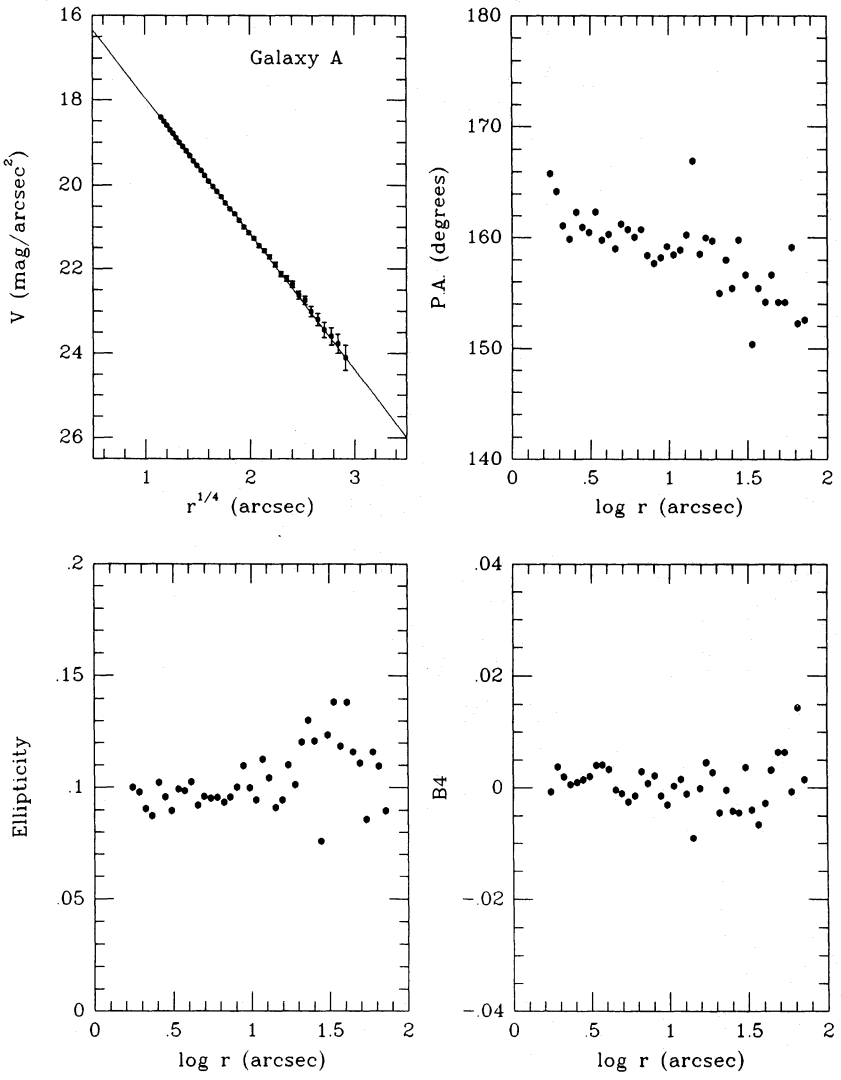

Fig. 2. Surface brightness profile, ellipticity, position angle, and B_4 component of the main galaxy in the simulated pair

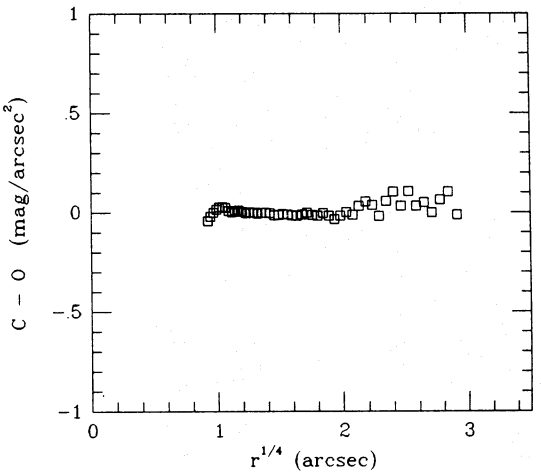

Fig. 3. Fitted de Vaucouleurs law minus measured surface brightness vs. semimajor axis for the main galaxy in the pair

Vaucouleurs law appear at intensity levels larger than 1.5% of the sky background.

Therefore, we believe that this method is a powerful tool to study the brightness profiles of pairs of elliptical galaxies. It can reveal strong isophote twists, gradients in ellipticity and isophote off-centering of the individual components of the pair.

3. The interacting galaxy pairs associated with B2 0034+25 and B2 0206+35

In this section, we discuss the results of the photometric analysis described above as applied to the galaxies B2 0034+25 and B2 0206+35 and their companions. We present profiles of ellipticity, position angle, normalized Fourier coefficients B_3 and B_4 and surface brightness as a function of semimajor axis. Apparent and absolute magnitudes as well as effective radii and effective surface brightness for the galaxies are listed in Table 2. A value of $H_0 = 75\ \mathrm{km\,s^{-1}\,Mpc^{-1}}$ is used throughout this paper.

3.1. *B2 0034+25*

This radio galaxy shows a wide angle tail morphology with a double jet (P.A. = 90°) of mean surface brightness at 1.4 GHz of 0.15 mJy arcsec^{-2} (Parma et al. 1987). It is located in projection near the center of the Zwicky open cluster 0034.4+2532 and on the POSS prints it appears to be the third brightest member of the cluster (Ekers et al. 1981). Figure 4 shows a contour map of the V image of B2 0034+25. The optical counterpart of the radio source is the brightest elliptical galaxy near the field center ($m_V = 13.35 \pm 0.07$ corresponding to an absolute magnitude $M_V = -22.19 \pm 0.07$). Its nearest companion ($m_V = 15.33 \pm 0.08$, corresponding to an absolute magnitude of -20.21 ± 0.08) is located to the SE at a projected distance of 26 kpc (44″). The companion shows an extension towards the NE and a dust lane crossing the central part at P.A. 44°.

Following the procedure explained in Sect. 2.3, an elliptical model of the main galaxy was constructed from the elliptical fit parameters and subtracted from the original image. Then a similar procedure was carried out for the companion galaxy. The resulting residual image, where both elliptical models have been subtracted, is shown in Fig. 5. The positions of the nuclei of the main galaxy and its nearby companion are marked by the letters A and B, respectively. Near the nucleus of the main galaxy cross-like residual features are seen, which are due to high non-ellipticities of the inner ($\leq 10''$) isophotes. At a distance of 11″, a faint object ($m_V \sim 20.9$) resembling a galaxy is detected towards the E of the main galaxy. No optical counterpart of the radio jet is detected brighter than the limiting surface brightness level of ~ 26 mag arcsec^{-2}.

Near the nucleus of the companion galaxy the fit is affected by the presence of the dust lane, producing positive residuals parallel to it. Further out towards the NE and to the N some extensions are present, which we identify as tidal tails.

We made a second model subtraction of the main galaxy masking out the brightest arms of the residual cross-like feature (at P.A. = 162°). The new residual image shows only residuals in P.A. 162°, aligned with the major axis of the main galaxy. Such feature can be interpreted as a stellar disk, which is nearly perpendicular to the radio axis (González-Serrano & Pérez-Fournon 1989). This demonstrates that the EW features seen in Fig. 5 near the nucleus are an artifact of the first fit. In Fig. 6 we represent the main isophote parameters and brightness profile resulting from the second fit. Ellipticity and $\cos 4\theta$ profiles from the first fit are also shown for comparison. The brightness profile is well fitted by a de Vaucouleurs law (straight line in Fig. 6) from about 6″ to 60″ from the nucleus in a range of 4 magnitudes. The corresponding effective surface brightness and radius are $\mu_e = 23.04$ mag arcsec^{-2} and $r_e = 26.5$ kpc respectively. The position angle of the major axis shows a very high twist, of approximately 65°, from the inner parts, where it coincides with the orientation of the stellar disk (162°), to the external regions where it is oriented towards the companion. The high positive $\cos 4\theta$ component and the high ellipticity in the first fit compared with the second one are caused by the presence of the disk. The brightness profile of galaxy A shows a point-like nuclear source above the extrapolation of the de Vaucouleurs law fitted to the outer parts.

In Fig. 7 we present the same parameters for the companion galaxy. The effective surface brightness and radius, as obtained from the fit to a de Vaucouleurs law, are $\mu_e = 21.31 \pm 0.11$ mag arcsec^{-2} and $r_e = 2.6 \pm 0.12$ kpc respectively. Galaxy B shows an isophote twist of 30° in the direction of the main galaxy. The ellipticity and $\cos 4\theta$ component in the inner parts are strongly affected by the dust lane.

Table 2. Photometric parameters of the galaxies and their companions

		m_V	M_V	μ_e	r_e (kpc)
B2 0034+25	A	13.35	−22.19	23.04	26.5
	B	15.33	−20.21	21.31	2.6
B2 0206+35	A	12.89	−23.00	—	—
	B	15.06	−20.80	20.20	1.66

3.2. *B2 0206+35*

B2 0206+35 (UGC 1651, 4C35.03; $z = 0.0375$ [Colla et al. 1975]) belongs to the Zwicky cluster 0216.0+3625 (medium compact).

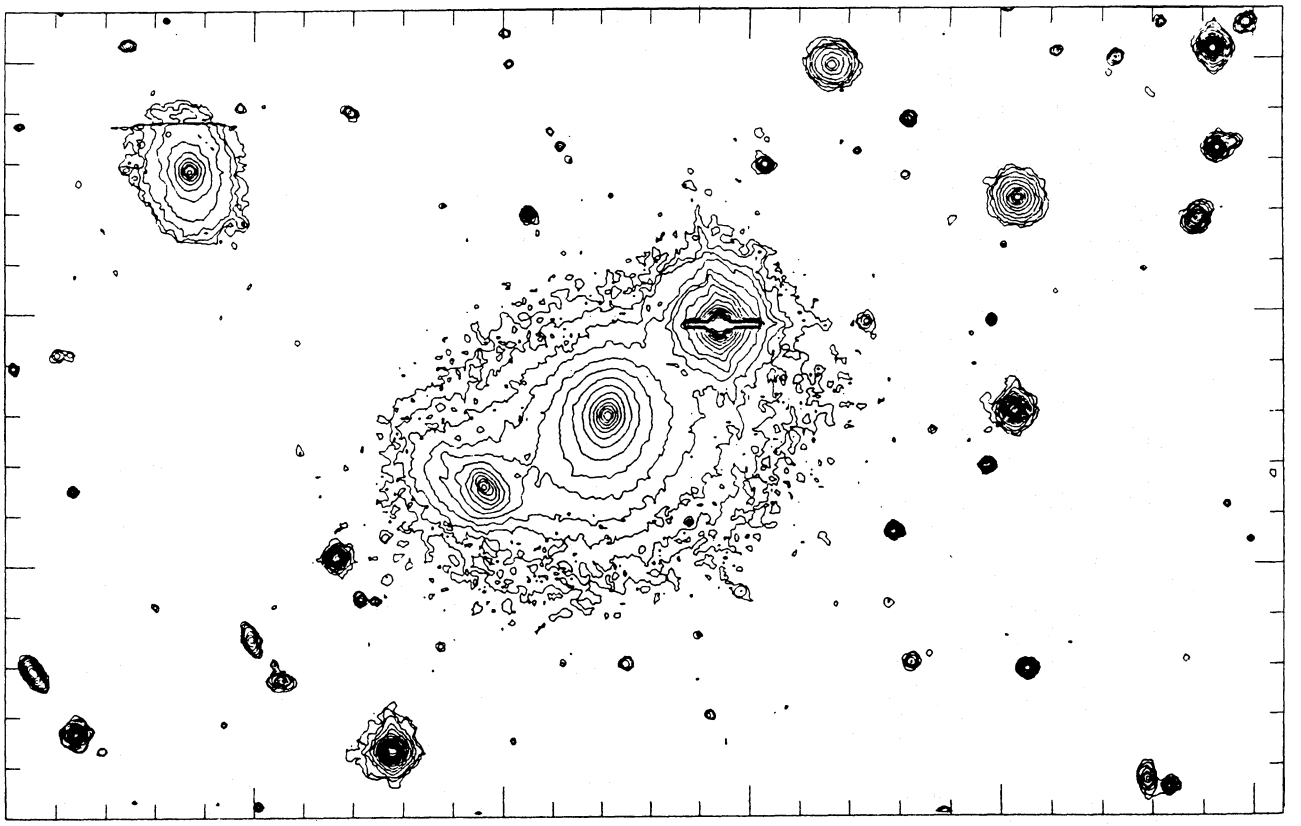

Fig. 4. Contour map of B2 0034+25 in the V filter. The optical counterpart of the radio source is the galaxy near the center of the field. North is up and east is to the left. Lower contour corresponds to 25 mag arcsec^{-2}, and the interval between contours is 0.5 mag. The separation between tick marks corresponds to 14″.8 (9.2 kpc). The star to the NW is saturated

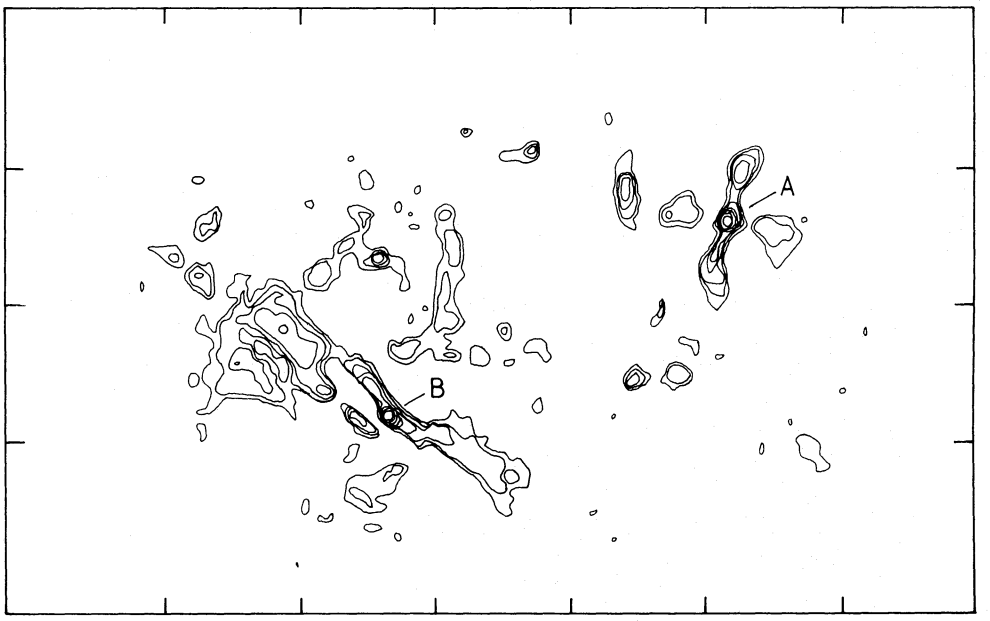

Fig. 5. Contour map of the residual image after subtracting the galaxy models of B2 0034+25 its SE companion. Letters A and B mark the position of the nuclei of both galaxies. First contour corresponds to 25.9 mag arcsec^{-2}, and the interval between contours is 0.5 mag. Oreintation scale are as in Fig. 4

At 1.4 GHz this source shows a double jet in the NW-SE direction with total extension of 33″ (24 kpc) to the NW and 34″ (24.7 kpc) to the SE (Parma et al. 1987). The mean surface brightness at this frequency of the NW and SE jets is 1.2 and 0.5 mJy arcsec^{-2}, respectively (Parma et al. 1987). Figure 8 shows a contour map of our V image. The brightest galaxy located at the field center is the optical counterpart of B2 0206+35. The total magnitude is $m_V = 12.89 \pm 0.07$ corresponding to $M_V = -23$

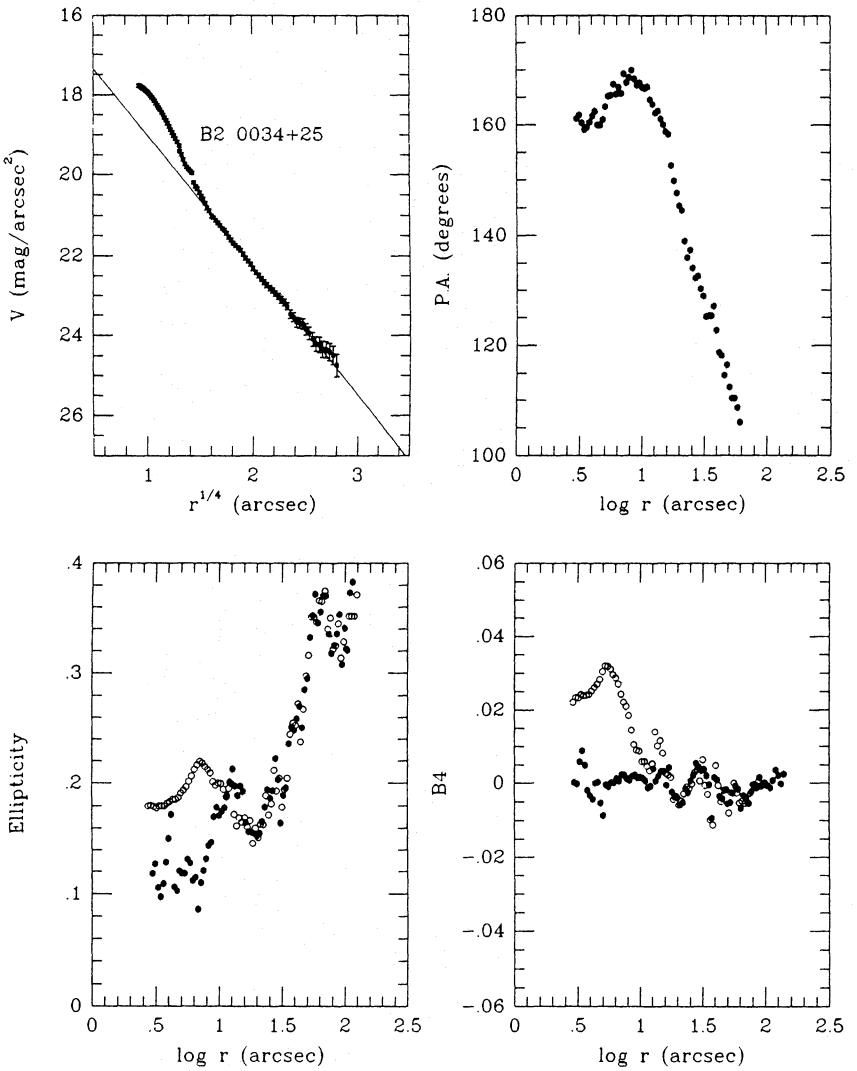

Fig. 6. Brightness profile isophote parameters of B2 0034+25 vs. semimajor axis. Empty filled circles in ellipticity and cos 4θ component represent the first and second fit, respectively (see text). The line represents the best fit to the de Vaucouleurs law

± 0.07. At a projected distance of 31 kpc (43 arcsec) in P.A. 110° there is a smaller galaxy with $m_V = 15.06$ ($M_V = -20.8$). Hereafter we will refer to the main galaxy and its companion as galaxy A and B, respectively.

Non-elliptical isophotes and a strong isophote twist are evident in the contour map. Therefore, we expect significant values of the high order (3rd and 4th) Fourier coefficients. Near the center the isophotes are very elongated ($\varepsilon = 0.3 - 0.4$) at P.A. 153°, suggesting the presence of a secondary nucleus, a disk or an inner dust lane. The latter was proposed by Battistini et al. (1980). The resolution of our image (FWHM = 1.″3) does not allow us to decide between the two possibilities. In Fig. 9 we show a contour map of the residual image resulting from the subtraction of an elliptical model of galaxy A from the original V image. Since the original image is clearly not elliptical, positive and negative residuals are expected, but Fig. 9 shows that only positive residuals exist, these concentrate in a wide region between P.A. 80′ and 175° with total extension 18″ (13 kpc), about half the projected distance to the companion. The peak in surface brightness of this region is located 2″ from the nucleus at P.A. 142°. The radio jet has a knot 4″ from the nucleus in P.A. 130°. Assuming that the optical and radio nuclei coincide, the optical "knot" does not represent the optical counterpart of the radio knot.

The companion galaxy is rather spherical in shape, except for a faint structure of total extension of 26″ (19 kpc) at P.A. 110°, opposite to the P.A. of the main galaxy from the companion. This feature resembles a tidal tail.

The best-fit ellipse brightness profiles and parameters of galaxies A and B are shown in Figs. 10 and 11, respectively. The bump in the brightness profile of galaxy A is probably caused by the source located 2″ from the nucleus. The position angle presents a strong twisting from the inner parts (P.A. 153°) to the external parts where the major axis is aligned with the direction towards the companion (P.A. 110°). The high B_3 term is indicative of the triangular shape of the isophotes which can be directly appreciated in the original image (Fig. 8). Peletier (1989) (and references therein) found a number of elliptical galaxies with significant cos 3θ terms which he attributes to the presence of dust. As we noted before, Battistini et al. (1980) reported an inner dust lane in this galaxy. However, the B_3 component is appreciable up to $\sim 20''$ from the nucleus and it may be the effect of a strong gravitational interaction with the SE companion.

Galaxy B follows a de Vaucouleurs law in the inner parts but shows excesses above the extrapolation of the inner fitted profile in the external regions starting at a level of 24 mag arcsec^{-2} and semimajor axis of 7″ (5 kpc). The best-fit profile parameters are

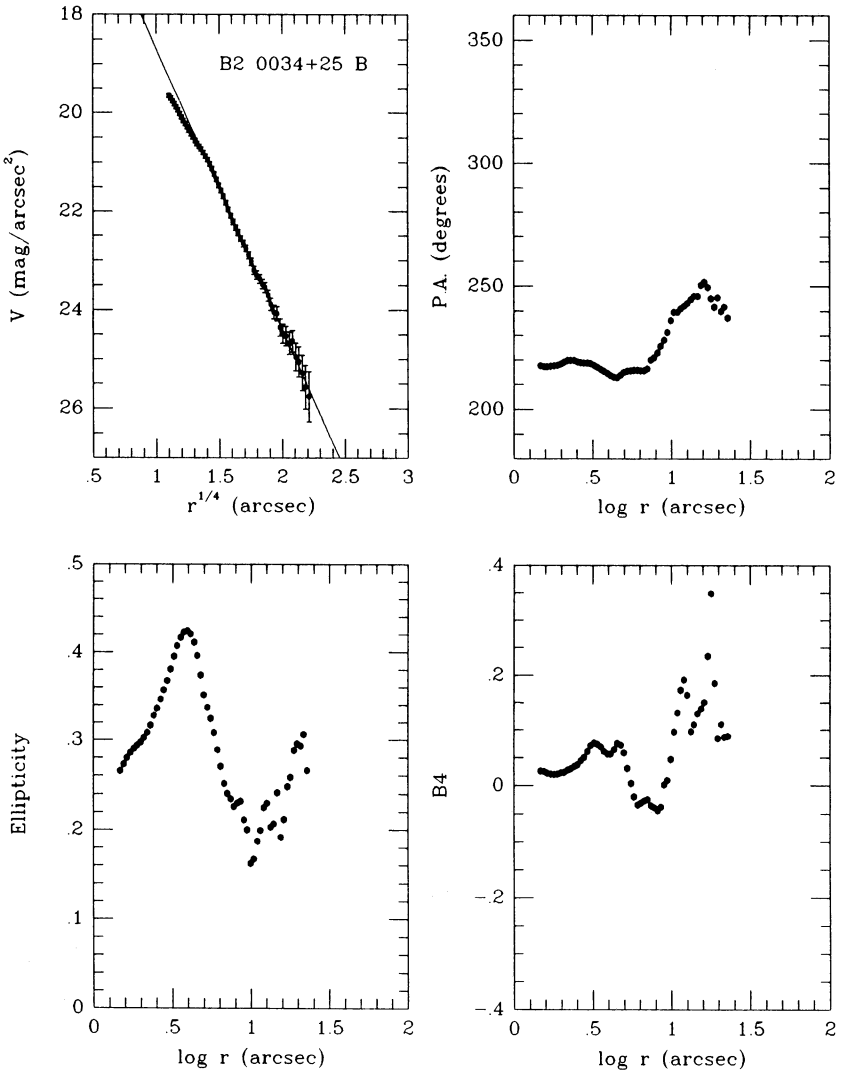

Fig. 7. Same as Fig. 6 for the companion galaxy of B2 0034+25

$\mu_e = 20.20 \pm 0.04$ mag arcsec^{-2} and $r_e = 1.66 \pm 0.03$ kpc. The isophote parameters are affected by the NW-SE extensions.

We have found off-centering of the outer isophotes in the main galaxy and its companion in both pairs of galaxies. The relative off-centering of B2 0034+25 and B2 0206+35 and their companions are represented in Fig. 12. The main galaxies have $\delta/a \sim 20\%$ and their companions have $\delta/a \sim 30\%$ at $a \sim 20$ kpc corresponding to maximum measured off-centering distances δ of 5–6 arcsec (3–5 kpc).

4. Discussion

4.1. Optical morphology

The optical structure of the radiogalaxies B2 0034+25 and B2 0206+35 indicates that they are interacting with their companions. Both main and companion galaxies show strong isophote twists. The outer isophotes tend to be aligned with the direction of their respective neighbours. The geometry of elliptical galaxies is known to present a dependence with radius which suggests that they might be triaxial systems (Williams & Schwarzschild 1979a, b; Leach 1981). The origin of the triaxial aspect may represent tidal disturbances or intrinsic structures. Kormendy (1982) and di Tullio (1979) stressed the point that geometry changes are related to the presence of companions, suggesting an effect of tidal interactions. The features observed in B2 0034+25 and B2 0206+35 are clear indicators of this type of phenomena.

The feature resembling a tidal tail, observed close to the companion of B2 0034+25, as well as other faint extensions revealed in the residual image (see Fig. 5), are also indicative of an on-going encounter. Similar structures are seen in B2 0206+35 and its companion. In this case, the high non-ellipticities and the anomalous brightness profile of the main galaxy are also probably related to a close encounter. In the case of B2 0206+35 there is an additional tracer of gravitational interaction between the galaxies. The brightness profile of galaxy B is well fitted by a $r^{1/4}$ law in the inner parts, while in the outer regions the emission is above the extrapolation of the de Vaucouleurs profile. Aguilar & White (1986) analysed the evolution of the brightness profile of a perturbed spherical galaxy during a close encounter with another system. The core of strongly bound particles moves away from the center of mass of the outer particles. The result is that the inner parts follow the $r^{1/4}$ law but with decreasing effective radius during the encounter. In the external parts the profile presents an excess over the de Vaucouleurs law fitted to the

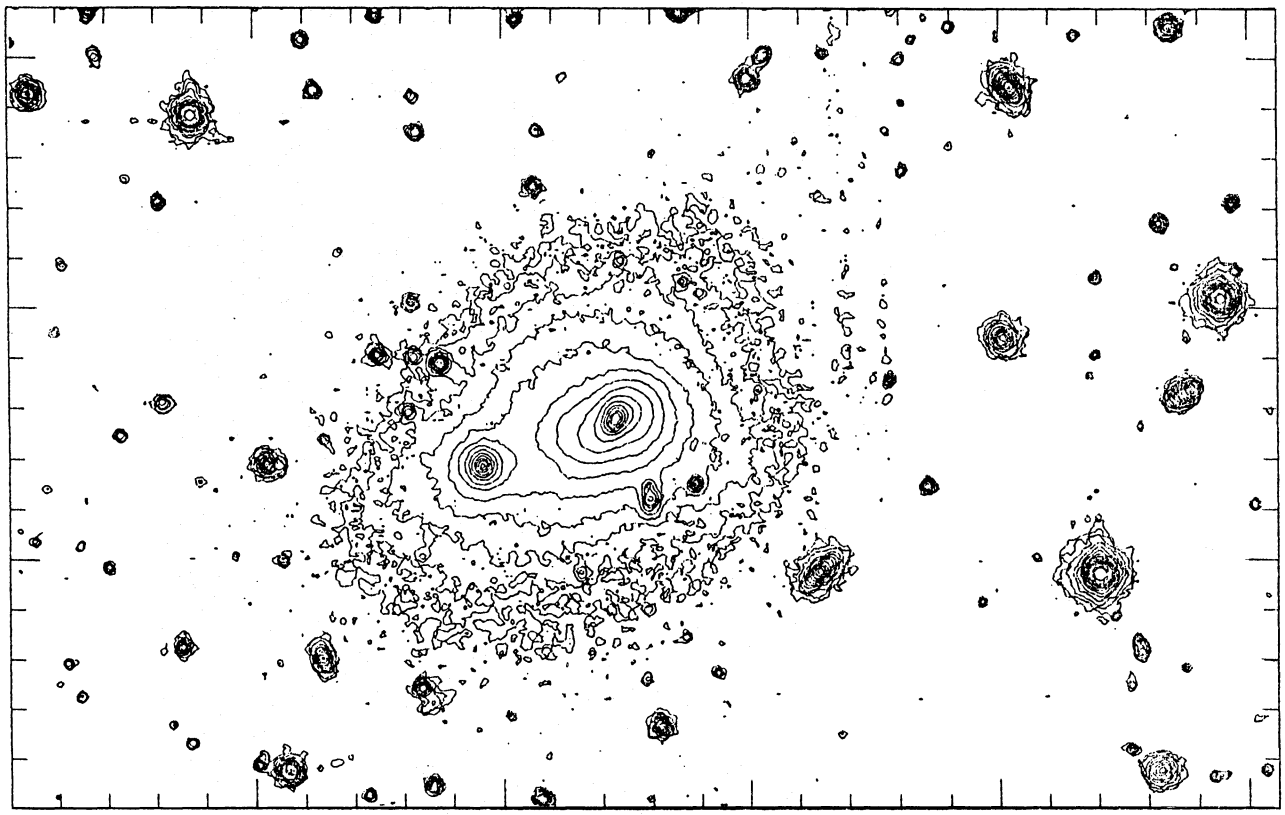

Fig. 8. Contour map of B2 0206+35 in the V filter. The optical counterpart of the radio source is the bright galaxy near the center of the field. First contour corresponds to 25 mag arcsec^{-2}, and the interval between contours is 0.5 mag. Orientation and scale are as in Fig. 4

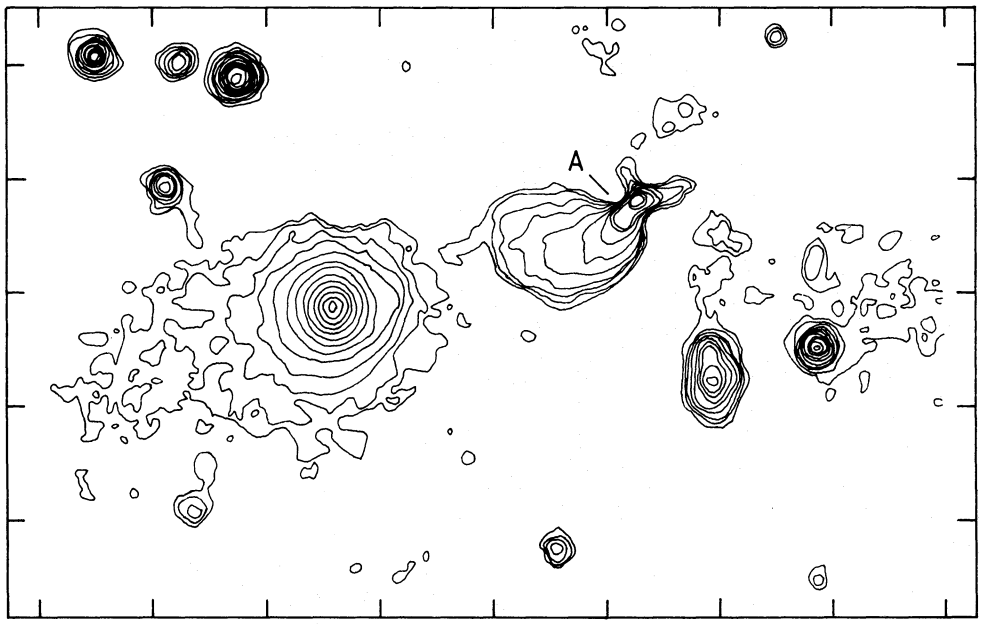

Fig. 9. Contour map of the residual image after subtraction of the galaxy model to B2 0206+35. First contour represents 25 mag arcsec^{-2}, and the interval between contours is 0.5 mag. A marks the nucleus of B2 0206+35

central parts. The radius where the excess starts does not depend on encounter parameters and the dynamical time at the distance where the boundary lies is equal to the time elapsed since the encounter. From the profile parameters of galaxy B we can estimate that the time since the closest approach is $2.4\,10^8 \times (M/L)^{-1/2}$ years, where M/L is the mass-to-light ratio of the galaxy. For the B2 0034+25 pair, where such excesses are not observed, we estimate that the encounter time is larger than $10^9 \times (M/L)^{-1/2}$ yr.

The strong off-centering of the outer isophotes found in both pairs of galaxies is most likely related to their mutual interaction (Lauer 1988). The larger relative isophote shifts occur in the

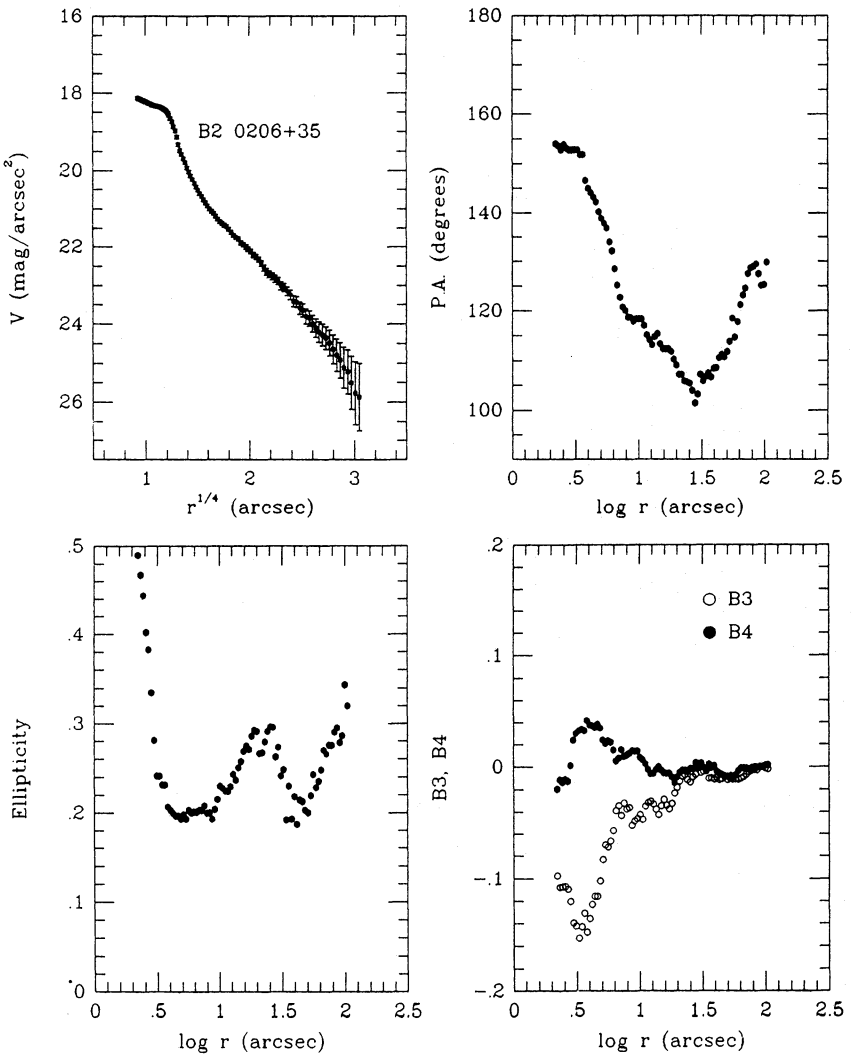

Fig. 10. Brightness profile isophote parameters of B2 0206+35 vs. semimajor axis

smaller galaxies of the pairs. This effect has also been found in a sample of nearby paired elliptical galaxies (Davoust & Prugniel 1988).

Bender et al. (1987) found a correlation between isophote shapes and radio emission in elliptical galaxies. Objects showing pointed isophotes are in general radio quiet and elliptical galaxies with box-shaped isophotes are frequently radio loud. The $\cos 4\theta$ in B2 0034+25 is less than 0.5% of the isophote intensities. After removing the disk component in B2 0034+25 there is not a significant boxy shape in the isophotes. In B2 0206 +35 the B_4 component is positive in the inner parts and it is related to the tidal tail feature detected and to the bright point source located 2″ to the SE. The B_3 component, probably originated by the interaction with the companion galaxy, is dominant in this galaxy.

If the presence of boxy isophotes is related to radio activity, B2 0034+25 seems to be an example violating the correlation found by Bender et al. (1987). Several possibilities can be drawn: (1) it could be projection effect in a similar way as it is for a disk component, (2) it could be a redshift-dependent phenomenon (note that most of the galaxies in the sample of Bender et al. are a factor $\gtrsim 3$ closer than B2 0034+25), or (3) it is not a regular E-disk galaxy being the interaction event the dominant factor in determining the isophote shapes.

An interesting feature in B2 0034+25 is the presence of a point-like nuclear source above the extrapolation of the de Vaucouleurs law fitted to the outer parts. This peak in the surface brightness profile could be the non-thermal optical counterpart of the radio nucleus or represent a massive nuclear stellar cluster. An alternative explanation is that it represents the remnant of a merged galaxy which has settled in the center of the potential well of the radio galaxy. González-Serrano & Pérez-Fournon (1989) have suggested that the disk component detected in the inner parts of B2 0034+25 is the signature of a cannibalized galaxy. Numerical simulations of mergers (Balcells 1989) show that if the smaller galaxy is denser, the central surface brightness of the remnants are dominated by the secondary material, and the brightness profile of the merger will show excesses in the central parts.

4.2. Radio-to-optical spectral index of the jets

Bicknell et al. (1990) present surface brightness profiles along the 23 jets in a sample of B2 radio sources associated with intermediate redshift galaxies. Both radio sources studied in this paper are included in the Bicknell's sample. At the frequency of 1.4 GHz the W jet in B2 0034+25 has a surface brightness ranging from 2 mJy arcsec^{-2} at 2″ to 0.08 mJy arcsec^{-2} at 20″.

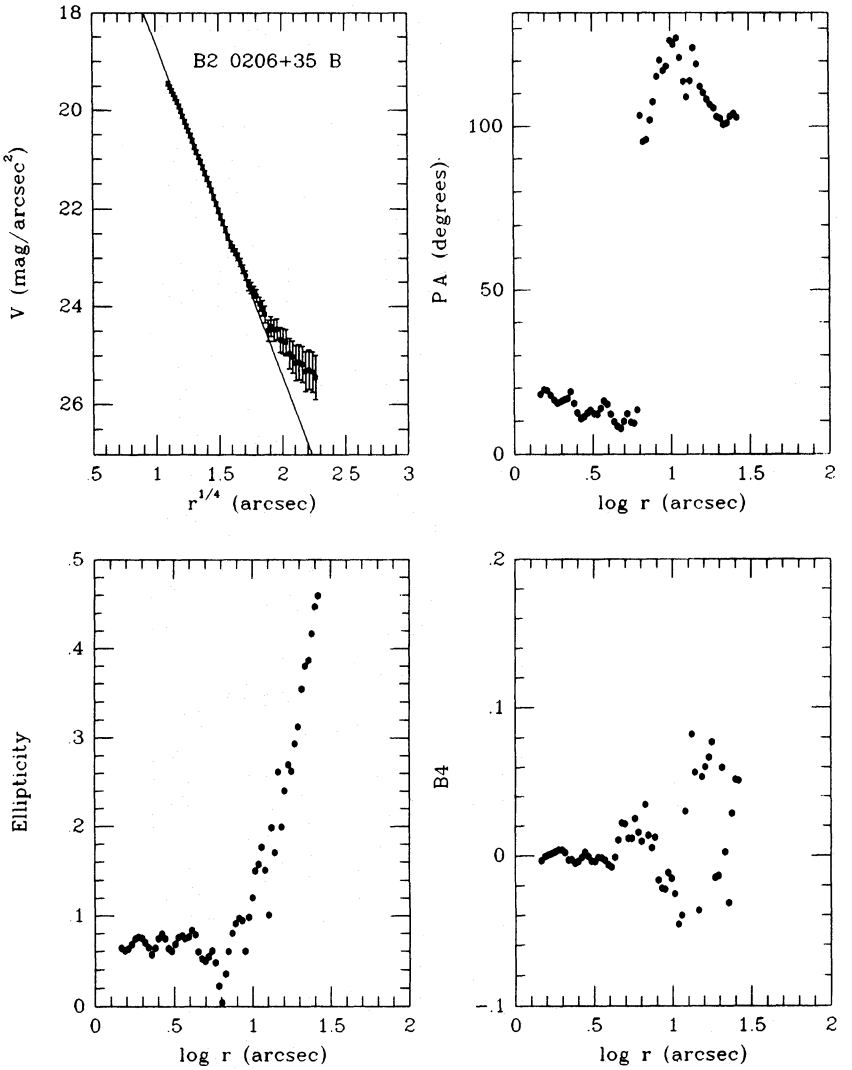

Fig. 11. Same as Fig. 10 for the companion galaxy of B2 0206+35. The line is the best fit to the de Vaucouleurs law

The surface brightness of the E jet is 3 mJy arcsec^{-2} at 2″ and 0.045 at 30″. The E and W jets in B2 0206+35 have surface brightness of 8 and 30 mJy arcsec^{-2} at 2″, respectively. The corresponding values at 20″ are 1.5 and 1 mJy arcsec^{-2}, respectively.

No optical counterparts of the jets are detected in the residual image of B2 0034+25. In the case of B2 0206+35, the spatial coincidence between the extended residuals detected and the SE radio jet, makes difficult to detect its optical counterpart in the inner parts.

Our 3σ detection limit in the outer parts of the galaxies is $\mu_V \sim 26$ mag arcsec^{-2} which corresponds to ~ 0.14 μJy arcsec^{-2}. In the inner parts of the galaxies the detection limit decreases by 1 magnitude because the higher brightness of the galaxy increases the Poisson noise. Taking this fact into account, we can put the following lower limits to the radio-to-optical spectral indices $\alpha (S_\nu \propto \nu^{-\alpha}$, where S_ν is the flux density at frequency ν) of the jets in B2 0034+25 and B2 0206+35:

— The spectral index in the central parts ($\sim 2''$) is higher than 0.7 for both jets in B2 0034+25. In the outer parts ($\gtrsim 20''$) the limits are 0.4 and 0.5 for the E and W jet, respectively. Since the spectral index at radio wavelengths is unknown, we compare our estimated values with the spectral indices of the M87 jet. Owen et al. (1980) obtain a spectral index of 0.6 between 6 and 2 cm for the jet. Assuming this value for the jets in B2 0034+25, our limit for the spectral index in the inner parts is consistent with a steepening of the spectrum at high frequencies.

— For the external parts of both jets in B2 0206+35 we estimate a lower limit for the spectral index of 0.7 between 1.4 GHz and V. In the inner parts of the NW jet the radio-to-optical spectral index is higher than 0.8 while for the SE jet the spectral index is higher than 0.9. Morganti et al. (1987) give values for the spectral indices of the jets in B2 0206+35 between 4.8 and 1.4 GHz. For the inner regions of the jets they measured a spectral index of 0.6. The values are 0.9 and 0.96 in the external parts of the NW and SE jets, respectively. Again, these values indicate a steepening of the spectra of the jets in the central parts. In the external ones, as in B2 0034+25, our lower limit of the spectral indices do not allow us to be conclusive.

We note that owing to the large difference between the radio and optical frequencies, the errors in the spectral indices are low and therefore, increases of 0.1 in the spectral indices are significative. We can conclude that an increase of the spectral index is present in the inner parts of the jets in B2 0034+25 and B2 0206+35 being the declining of the spectra located at frequencies below $5.6\,10^{14}$ Hz. The cut-off is related to the electron energy

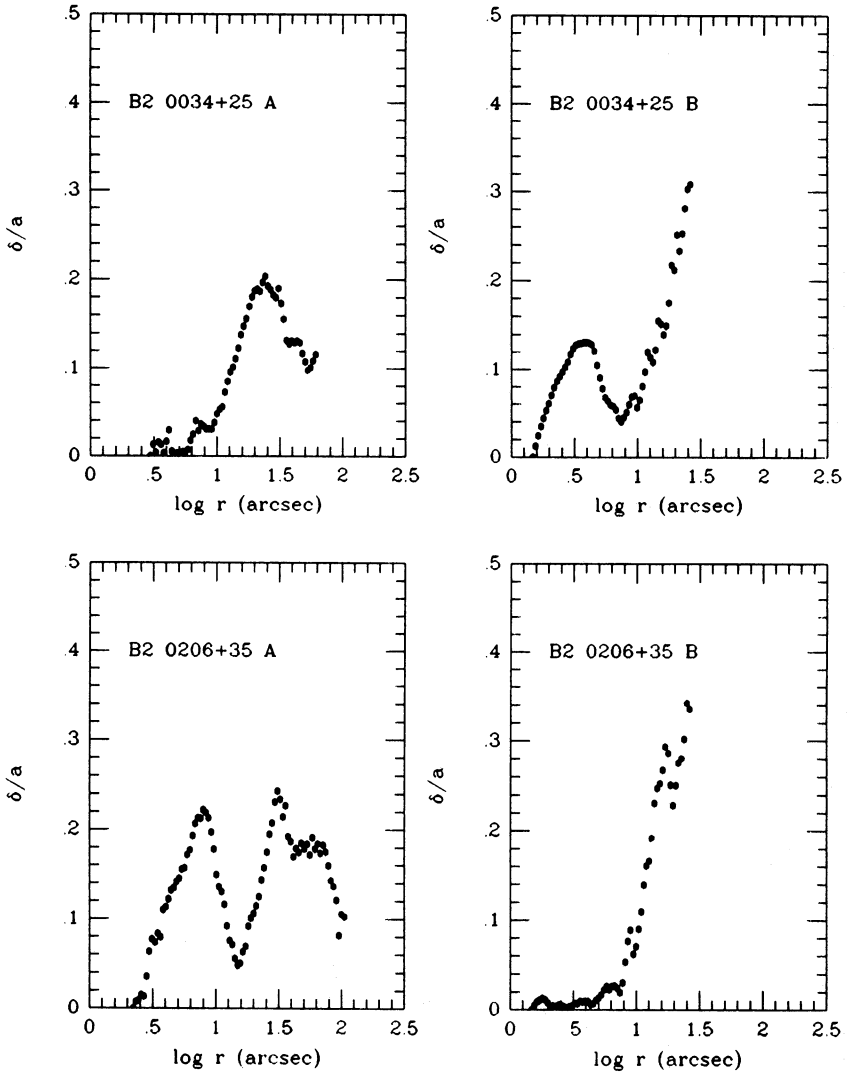

Fig. 12. δ/a deviations along the semimajor axis of the four galaxies B2 0034+25 A, B, and B2 0206 +35 A, B

distribution and could be intrinsic to acceleration processes (Biermann & Strittmatter 1987; Pérez-Fournon et al. 1988).

4.3. Collimation of the radio jets: hot gas around low luminosity radio galaxies

Bicknell et al. (1990) have fitted a semi-empirical turbulent jet model to their sample of 23 jets. They assume hydrostatic isothermal atmospheres, and derive core radii of about 1 kpc consistent with typical values for cD galaxies. However, the determination of the jet properties (velocity, Mach number) depend upon the variation of pressure within the galactic atmospheres. For B2 0034+25 the galactic atmosphere parameters resulting from the fit to the jets agree on both sides of the nucleus. Out of 8 sources with two sided jets in Bicknell's sample, the galactic atmospheres parameters agree on both sides of the nucleus in 5 cases. In two of the three remaining cases (B2 1450+28 and B2 1752+32) and model parameters disagree. For the third galaxy, B2 0206+35, Bicknell et al. (1990) are inconclusive. They claim that the fitted atmosphere parameters on both sides of the nucleus are consistent with each other, but their Fig. 2 shows very different pressure profiles for the two jets.

A detailed study of B2 0206+35 has been carried out by Morganti et al. (1987). The two jets are quite different, both in expansion rates and brightness distribution. While the NW jet shows a rather constant spreading rate and decollimates at about 20″ from the nucleus, the SE jet presents a high expansion rate and decollimates at 10″. In the following we attempt to link the peculiar properties of the SE radio jet in B2 0206+35 with the distorted optical morphology and evidence of strong gravitational interaction of the main galaxy and its companion.

CCD imaging of a extensive sample of B2 radio-jet galaxies shows that a large fraction appear to be gravitationally interacting with nearby companions (González-Serrano 1989; González-Serrano & Pérez-Fournon 1989; Colina & Pérez-Fournon 1990a, b). Thus the collisions may contribute to the heating of the hot gas and introducing asymmetries in its spatial distribution. Unfortunately, the two sources are not included in the sample of B2 radio galaxies observed with the Einstein or EXOSAT Observatories. By comparison with the X-ray properties of 22 radio galaxies observed with Einstein (Morganti et al. 1988) and of normal giant ellipticals (Biermann & Kronberg 1983) we expect the presence of hot gas around these galaxies which can determine the jet spreading rates. The distribution of

X-ray emission around the radio galaxies discussed by Morganti et al. (1988) shows many types of morphology. In some cases the X-ray emission peaks at the position of the radio source, but in other cases the peak is displaced from the radio core.

The difference in the pressure profiles determined by Bicknell et al. (1990) for the SE and NW jets of B2 0206+35 indicates that the pressure profile of the external medium confining the SE jet is not the same as for the NW jet. We suggest that this difference is originated by the heating of the gas caused by the companion galaxy intruding in the atmosphere of B2 0206+35.

Acknowledgements. We wish to thank the support provided by Dr. E. Brinks during the observations. We also thank M. Balcells, T.S. van Albada, and the referee, R. Bender, for useful comments. JIGS was supported by the IAC and by a fellowship of the Spanish Ministry of Education and Science. Part of this work was done at the Kapteyn Astronomical Institute in Groningen.

References

Aguilar L.A., White S.D.M., 1986, ApJ 307, 97
Balcells M., 1989, Ph.D. Thesis, University of Wisconsin-Madison
Battistini P., Bonoli F., Silvestro S., Fanti R., Gioia I., Giovannini G., 1980 A&A 85, 101
Baum S.A., Heckman T.M., 1989a, ApJ 336, 681
Baum S.A., Heckman T.M., 1989b, ApJ 336, 702
Bender R., Möllenhoff C., 1987, A&A 177, 71
Bender R., Döbereiner S., Möllenhoff C., 1987, A&A 177, L53
Bender R., Surma P., Döbereiner S., Möllenhoff C., Medejsky R., 1989, A&A 217, 35
Bicknell G.V., de Ruiter H.R., Fanti R., Morganti R., Parma P., 1990, ApJ 354, 98
Biermann P.L., Kronberg P.P., 1983, ApJ 268, L69
Biermann P.L., Strittmatter P.A., 1987, ApJ 322, 643
Bridle A.M., Perley R.A., 1984, ARA&A 22, 319
Cawson M., 1983, Ph.D. thesis, University of Cambridge
Christian C.A., Adams M., Barnes J.V., Butcher H., Hayes D.S., Mould J.R., Siegel M., 1985, PASP 97, 363
Colina L., Pérez-Fournon I., 1990a, ApJS 72, 41
Colina L., Pérez-Fournon I., 1990b, ApJ 349, 45
Colla G., Fanti C., Fanti R., Gioia I., Lari C., Lequeux J., Lucas R., Ulrich M.H., 1975, A&AS 20, 1
Davoust E., Prugniel P., 1988, A&A 201, L30
Ekers R.D., Fanti R., Fanti C., Parma P., 1981, A&A 101, 194
Fanaroff B.L., Riley J.M., 1974, MNRAS 167, 31P
Fanti R., Gioia I., Lari C., Ulrich M.H., 1978, A&AS 34, 341
Fosbury R.A.E., 1989, in: Extranuclear Activity in AGN, ESO Workshop, eds. E.J.A. Meurs, R.A.E. Fosbury, ESO, Garching, p. 169
González-Serrano J.I., 1989, Ph.D. Thesis, University of La Laguna
González-Serrano J.I., Pérez-Fournon I., 1989, ApJ 338, L29
Heckman T.M., Smith E.P., Baum S.A., van Breugel W.J.M., Miley G.K., Illingworth G.D., Bothum G.D., Balick B., 1986, ApJ 311, 526
Huchra J.P., 1977, ApJS 35, 171
Jedrzejewski R.I., 1987, MNRAS 226, 747
Kormendy J., 1982, in: Morphology Dynamics of Galaxies, eds. L. Martinet, M. Mayor, Geneva Obs., Geneva, p. 113
Lauer T.R., 1988, ApJ 325, 49
Leach R., 1981, ApJ 248, 485
Lilly S.J., Prestage R.M., 1987, MNRAS 225, 531
Longair M.S., Seldner M., 1979, MNRAS 189, 433
Morganti R., Fanti C., Fanti R., Parma P., de Ruiter H.R., 1987, A&A 183, 203.
Morganti R., Fanti R., Gioia I., Harris D.E., Parma P., de Ruiter H.R., 1988, A&A 189, 11
Nieto J.-L., Bender R., 1989, A&A 215, 266
Owen F.N., Hardee P.E., Bignell R.C., 1980, ApJ 239, L11
Parma P., Fanti C., Fanti R., Morganti R., de Ruiter H.R., 1987, A&A 181, 244
Peletier R.F., 1989, Ph.D. Thesis, University of Groningen
Pérez-Fournon I., Colina L., González-Serrano J.I., Biermann P.L., 1988, ApJ 329, L81
Prestage R.M., Peacock J.A., 1988, MNRAS 230, 131
Savage B.D., Mathis J.S., 1979, ARA&A 17, 73
Smith E.P., Heckman T.M., 1989a, ApJS 69, 365
Smith E.P., Heckman T.M., 1989b, ApJ 341, 658
Stocke J., 1979, ApJ 230, 40
di Tullio G.A., 1979, A&AS 37, 591
Williams T.B., Schwarzschild M., 1979a, ApJ 227, 56
Williams T.B., Schwarzschild M., 1979b, A&AS 41, 209